

阻抗劈绕射对破碎波后向散射特性的影响

张肖肖 吴振森 苏翔

Effects of impedance wedge diffraction on backscattering from breaking waves

Zhang Xiao-Xiao Wu Zhen-Sen Su Xiang

引用信息 Citation: *Acta Physica Sinica*, 65, 214101 (2016) DOI: 10.7498/aps.65.214101

在线阅读 View online: <http://dx.doi.org/10.7498/aps.65.214101>

当期内容 View table of contents: <http://wulixb.iphy.ac.cn/CN/Y2016/V65/I21>

您可能感兴趣的其他文章

Articles you may be interested in

[基于交替隐式有限差分法的快速早期乳腺癌时域微波断层成像](#)

[Microwave tomography for early breast cancer detection based on the alternating direction implicit finite-difference time-domain method](#)

物理学报.2016, 65(14): 144101 <http://dx.doi.org/10.7498/aps.65.144101>

[一种内置条状金属板的双层金属腔体屏蔽效能的理论模型](#)

[An analytical model for shielding effectiveness of double layer rectangular enclosure with inner strip-shaped metallic plate](#)

物理学报.2016, 65(4): 044101 <http://dx.doi.org/10.7498/aps.65.044101>

[高浓度纤维增强材料介电特性计算方法](#)

[An approach to characterize dielectric properties of fiber-reinforced composites with high volume fraction](#)

物理学报.2016, 65(2): 024102 <http://dx.doi.org/10.7498/aps.65.024102>

[左手介质对谐振腔谐振频率的影响](#)

[Influence of left-handed material on the resonant frequency of resonant cavity](#)

物理学报.2015, 64(12): 124103 <http://dx.doi.org/10.7498/aps.64.124103>

[高增益相对论速调管放大器相位特性的模拟与实验研究](#)

[Simulation and experimental study of phase characteristics in high-gain relativistic klystron amplifier](#)

物理学报.2015, 64(8): 084102 <http://dx.doi.org/10.7498/aps.64.084102>

阻抗劈绕射对破碎波后向散射特性的影响*

张肖肖¹⁾ 吴振森^{1)2)†} 苏翔¹⁾

1)(西安电子科技大学物理与光电子工程学院, 西安 710071)

2)(西安电子科技大学信息感知技术协同创新中心, 西安 710071)

(2016年5月18日收到; 2016年6月21日收到修改稿)

海浪的破碎区会导致海面电磁散射特性发生很大改变, 导致海尖峰现象的产生。本文结合阻抗劈结构模型分析了劈绕射对破碎波后向散射特性的影响。首先利用基尔霍夫近似求解破碎波的物理光学场; 基于Maliuzhinets方法, 从波动方程及精确阻抗边界条件出发, 由谱函数的积分形式得到阻抗劈的一致性绕射系数, 结合物理光学绕射系数导出阻抗劈等效边缘电磁流; 利用边缘绕射场修正物理光学场, 得到考虑劈绕射效应的破碎波散射总场。数值结果表明, 阻抗劈的绕射场在Keller锥内出现HH极化大于VV极化的现象, 因此计入绕射场的影响会使得破碎波生长到临近坍塌阶段时, 小擦地角逆风观测出现总场的后向散射截面HH极化大于VV极化的现象, 说明劈绕射是造成海尖峰现象产生的原因之一。

关键词: 后向散射, 破碎波, 等效边缘电磁流, 阻抗劈

PACS: 41.20.-q, 42.25.Bs, 42.25.Dd

DOI: 10.7498/aps.65.214101

1 引言

海面电磁散射研究对海面目标探测、制导、识别具有十分重要的意义。高海情下, 浪涌间相互作用增强, 波浪的生长坍塌往往伴随破碎波的产生, 海浪的破碎区会造成电磁散射特性发生很大改变。大量试验与研究表明, 破碎波是海尖峰产生的最主要原因, 而且海尖峰特性与破碎波的生长期和坍塌期有关^[1–3]。

Kalmykov 和 Pustovoytenko^[4] 分析了小擦地角下的实测海面回波数据, 认为类似劈结构的波冠散射造成了散射系数的极化差异。Kwoh 和 Lake^[5] 采用几何绕射理论计算劈绕射, 并利用微扰法计算了张力波散射, 从而得到了含碎浪的海面散射。Lyzenga 和 Ericson^[6] 采用劈结构来近似碎浪, 将劈散射系数与海面散射系数相加得到统计意义上的总散射系数。Holliday 等^[7] 采用前后向迭代方法计算了劈的海面双站散射。罗伟等^[8] 利用几何绕射理论研究了二面角劈结构的散射, 并结合白冠

覆盖率建立海面破碎波复合模型, 分析了时变海面回波强度和多普勒谱。在破碎波的几何建模方面, 美国加州大学通过海洋动力学原理得到了破碎波形成的公式, 并使用计算机数值仿真得到了LONGTANK破碎波模型, 该模型被广泛应用到破碎波研究中^[9]; 李文龙等^[10]建立了卷浪模型, 在LONGTANK的基础上加入了时间参数并考虑了风速的影响, 分析了卷浪的散射幅值及时变多普勒频谱特性。

遗憾的是, 以上学者在处理劈问题时仅考虑了理想导体劈的情形, 阻抗劈相对于理想导体劈, 其电磁散射特性发生了很大变化, 因此理想导体劈并不能很好地反映实际介质海面。求解阻抗劈绕射所用的方法主要有两种: Maliuzhinets方法^[11] 和Wiener-Holff方法^[12]。这两种方法都是从严格的波动方程出发结合阻抗边界条件, 求出空间场积分表达式, 再经渐近处理得出一致绕射理论(uniform theory of diffraction, UTD)的解, 但只能解决特殊劈角或者特殊入射问题^[13]。吴良超等推导了一致

* 国家自然科学基金(批准号: 61471242)资助的课题。

† 通信作者。E-mail: Wuzhs@mail.xidian.edu.cn

性绕射系数的一种简洁表达式^[14], 并分析了阻抗劈中的等效边缘电磁流, 并未考虑电磁场之间的耦合作用^[15]. Lyalinov 等^[16]提出利用摄动法, 基于正入射和掠入射对谱函数进行展开, 利用修正傅里叶变换得到了谱函数展开系数. Yuan 和 Zhu^[17]基于摄动法进一步求解了任意入射、任意劈角阻抗劈的散射场. 李骥等^[18]利用数值匹配方法计算了各向异性阻抗劈散射系数, 余定峰等^[19]在此基础上利用绕射场修正物理光学场, 计算了含劈结构目标的散射.

本文计算了不同劈角阻抗劈的绕射场, 并分析了劈面阻抗对绕射场的影响, 利用等效边缘电磁流法计算了二面角阻抗劈的后向雷达散射截面(radar cross-section, RCS); 分析了含劈结构的LONTANK模型散射特性, 认为劈边缘引起等效电磁流的不连续, 导致了HH极化和VV极化散射的差异, 这为雷达对海杂波探测与评估体系提供了技术支撑.

2 基本理论

2.1 破碎波物理光学场

基于基尔霍夫近似的物理光学法是求解Helmholtz积分方程的近似方法, 设散射面 \mathbf{r} 处的法向矢量为 $\hat{\mathbf{n}}$, 水平极化矢量定义为 $\hat{\mathbf{h}} = \hat{\mathbf{n}} \times \hat{\mathbf{k}}_i / |\hat{\mathbf{n}} \times \hat{\mathbf{k}}_i|$, 垂直极化矢量为 $\hat{\mathbf{v}} = \hat{\mathbf{h}} \times \hat{\mathbf{k}}_i$, 则表面感应电磁流可以表示为(以下省略时间因子 $e^{j\omega t}$)

$$\begin{aligned} \mathbf{J}(\mathbf{r}') &= \frac{1}{\eta_0} [-(\hat{\mathbf{e}}_i \cdot \hat{\mathbf{h}})(\hat{\mathbf{n}} \cdot \hat{\mathbf{k}}_i)(1 - R_{HH})\hat{\mathbf{h}} \\ &\quad + (\hat{\mathbf{e}}_i \cdot \hat{\mathbf{v}})(\hat{\mathbf{n}} \times \hat{\mathbf{h}})(1 + R_{VV})] \\ &\quad \cdot E_0 e^{-jk\hat{\mathbf{k}}_i \cdot \mathbf{r}'}, \\ \mathbf{M}(\mathbf{r}') &= -[(\hat{\mathbf{e}}_i \cdot \hat{\mathbf{h}})(\hat{\mathbf{n}} \times \hat{\mathbf{h}})(1 + R_{HH}) \\ &\quad + (\hat{\mathbf{e}}_i \cdot \hat{\mathbf{v}})(\hat{\mathbf{n}} \cdot \hat{\mathbf{k}}_i)(1 - R_{VV})\hat{\mathbf{h}}] \\ &\quad \cdot E_0 e^{-jk\hat{\mathbf{k}}_i \cdot \mathbf{r}'}, \end{aligned} \quad (1)$$

其中, R_{HH} 和 R_{VV} 分别为水平和垂直 Fresnel 反射系数, k 和 η_0 为自由空间波数和波阻抗, 入射场为 $\mathbf{E}^i(\mathbf{r}') = \hat{\mathbf{e}}_i E_0 e^{-jk\hat{\mathbf{k}}_i \cdot \mathbf{r}'}$. 利用远场近似得到远区散射场

$$\begin{aligned} \mathbf{E}^s(\mathbf{r}) &= -j \frac{\omega \mu_0}{4\pi r} e^{-jk r} \iint_S d\mathbf{s}' \{ \mathbf{J}(\mathbf{r}') \\ &\quad - [\mathbf{J}(\mathbf{r}') \cdot \hat{\mathbf{k}}_s] \hat{\mathbf{k}}_s \} \end{aligned}$$

$$+ \sqrt{\frac{\varepsilon_0}{\mu_0}} [\mathbf{M}(\mathbf{r}') \times \hat{\mathbf{k}}_s] \} e^{jk\hat{\mathbf{k}}_s \cdot \mathbf{r}'} . \quad (2)$$

由于破碎波含有劈结构, 仅仅求解其表面的物理光学场是不够的, 还需要求解由劈引入的绕射效应, 具体过程见下节.

2.2 阻抗劈绕射场及劈绕射系数

平面波斜入射阻抗劈如图1所示. 根据Maxwell方程组, 自由空间中纵向电磁场满足标量Helmholtz方程:

$$\begin{aligned} \nabla_t^2 E_z + k^2 \sin^2 \beta E_z &= 0, \\ \nabla_t^2 H_z + k^2 \sin^2 \beta H_z &= 0. \end{aligned} \quad (3)$$

阻抗劈中两阻抗面的精确阻抗边界条件为

$$\begin{aligned} \frac{1}{\rho} \frac{(\eta_0 H_z)}{\partial \phi} &\mp jk \sin \beta \sin \theta_{0,n}^h(\eta_0 H_z) \\ &+ \cos \beta \frac{\partial E_z}{\partial \rho} = 0, \quad \phi = 0, n\pi, \\ \frac{1}{\rho} \frac{\partial E_z}{\partial \phi} &\mp jk \sin \beta \sin \theta_{0,n}^e E_z \\ &- \cos \beta \frac{\partial (\eta_0 H_z)}{\partial \rho} = 0, \quad \phi = 0, n\pi, \end{aligned} \quad (4)$$

式中 E_z, H_z 分别为纵向电场和纵向磁场; $\phi = 0$ 对应阻抗劈的面, $\phi = n\pi$ 对应阻抗劈的 n 面; β 为入射角与劈边夹角, 并有

$$\begin{aligned} \sin \theta_{0,n}^e &= \sin \beta (\eta_0 / Z_{0,n}), \\ \sin \theta_{0,n}^h &= \sin \beta (Z_{0,n} / \eta_0), \end{aligned} \quad (5)$$

$Z_{0,n}$ 代表两劈面的阻抗.

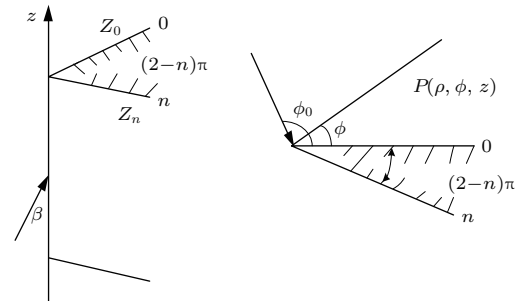


图1 平面波斜入射到阻抗劈示意图

Fig. 1. Impedance wedge with obliquely incident plane wave.

按照Maliuzhinet方法, 总场可表示为沿Sommerfeld路径的平面波谱积分形式:

$$\begin{bmatrix} E_z \\ \eta_0 H_z \end{bmatrix} = \frac{e^{-jkz \cos \beta}}{2\pi j} \int_\gamma S_{e,h} \left(\alpha - \phi + \frac{n\pi}{2} \right) \times e^{jk\rho \sin \beta \cos \alpha} d\alpha. \quad (6)$$

将(4)式代入(6)式经分部积分可得关于电磁场的耦合积分方程

$$\begin{aligned} & \int_{\gamma} e^{jk\rho \sin \beta \cos \alpha} (\sin \alpha \pm \sin \theta_{0,n}^h) S_h \left(\alpha \pm \frac{n\pi}{2} \right) \\ & + \cos \beta \cos \alpha S_e \left(\alpha \pm \frac{n\pi}{2} \right) d\alpha = 0, \\ & \int_{\gamma} e^{jk\rho \sin \beta \cos \alpha} (\sin \alpha \pm \sin \theta_{0,n}^e) S_e \left(\alpha \pm \frac{n\pi}{2} \right) \\ & + \cos \beta \cos \alpha S_h \left(\alpha \pm \frac{n\pi}{2} \right) d\alpha = 0. \end{aligned} \quad (7)$$

1) 基于正入射摄动法

Lyalinov 将谱函数表示为

$$\begin{aligned} S_{e,h}(\alpha) &= \Psi_{e,h}(\alpha) \sigma_{\phi_0}(\alpha) \\ &\times \sum_{m=0}^{\infty} \xi_{e,h}(\alpha) \cos^m \beta, \end{aligned} \quad (8)$$

式中, $\Psi_{e,h}(\alpha)$ 为马丢函数, $\sigma_{\phi_0}(\alpha)$ 为亚纯函数. 谱函数的零次项和一次项系数为

$$\xi_{e,h}^0(\alpha) = U_{e,h}^i / \Psi_{e,h}(n\pi/2 - \phi_i), \quad (9)$$

$$\begin{aligned} \xi_{e,h}^1(\alpha) &= -U_e^i \frac{j \sin(\alpha/n)}{4n\pi \Psi_e(n\pi/2 - \phi_0)} \\ &\times \left\{ \int_{-j\infty}^{j\infty} \frac{\cos t}{\cos(t/n)} \right. \\ &\times \frac{\Psi_e(n\pi/2 + t) - \Psi_e(n\pi/2 - t)}{(\sin t + \sin \theta_h^0) \Psi_h(n\pi/2 + t)} \\ &\times [\sigma_1(t, \alpha) - \sigma_1(t, n\pi/2 - \phi_0)] dt \\ &+ \int_{-j\infty}^{j\infty} \frac{\cos t}{\cos(t/n)} \\ &\times \frac{\Psi_e(n\pi/2 + t) - \Psi_e(-n\pi/2 - t)}{(\sin t + \sin \theta_h^n) \Psi_h(-n\pi/2 + t)} \\ &\times [\sigma_2(t, \alpha) - \sigma_2(t, n\pi/2 - \phi_0)] dt \end{aligned} \quad (10)$$

$$\begin{aligned} \xi_e^1(\alpha) &= -U_h^i \frac{j \sin(\alpha/n)}{4n\pi \Psi_h(n\pi/2 - \phi_0)} \\ &\times \left\{ \int_{-j\infty}^{j\infty} \frac{\cos t}{\cos(t/n)} \right. \\ &\times \frac{\Psi_h(n\pi/2 + t) - \Psi_h(n\pi/2 - t)}{(\sin t + \sin \theta_e^0) \Psi_e(n\pi/2 + t)} \\ &\times [\sigma_1(t, \alpha) - \sigma_1(t, n\pi/2 - \phi_0)] dt \\ &+ \int_{-j\infty}^{j\infty} \frac{\cos t}{\cos(t/n)} \\ &\times \frac{\Psi_h(n\pi/2 + t) - \Psi_h(-n\pi/2 - t)}{(\sin t + \sin \theta_e^n) \Psi_e(-n\pi/2 + t)} \end{aligned}$$

$$\left. \times [\sigma_2(t, \alpha) - \sigma_2(t, n\pi/2 - \phi_0)] dt \right\}, \quad (11)$$

式中

$$\sigma_l(t, \alpha) = \frac{\sin(t/n)}{\cos(t/n) + (-1)^l \sin(t/n)} \quad (l = 1, 2). \quad (12)$$

得到谱函数以后, 利用最陡下降法可以得到绕射场

$$\begin{bmatrix} E_z^d \\ \eta_0 H_z^d \end{bmatrix} = \frac{e^{-jk\rho \sin \beta} e^{-jkz \cos \beta} e^{-j\frac{\pi}{4}}}{2n\sqrt{2\pi k\rho \sin \beta}}$$

$$\begin{aligned} &\times \left\{ \begin{bmatrix} \Pi_e(\alpha_1) \\ \Pi_h(\alpha_1) \end{bmatrix} \times P_1 \right. \\ &\left. + \begin{bmatrix} \Pi_e(\alpha_2) \\ \Pi_h(\alpha_2) \end{bmatrix} \times P_2 \right\}, \end{aligned} \quad (13)$$

式中 $\alpha_1 = \pi + n\pi/2 - \phi$, $\alpha_2 = -\pi + n\pi/2 - \phi$. 且

$$\Pi_{e,h}(\alpha) = \Psi_{e,h}(\alpha) \sum_{m=0}^{\infty} \xi_{e,h}(\alpha) \cos^m \beta, \quad (14)$$

$$\begin{aligned} P_1 &= \cot \frac{\pi - (\phi - \phi_0)}{2n} \\ &\times F\{k\rho \sin \beta [1 + \cos(\phi - \phi_0)]\} \\ &- \cot \frac{\pi - (\phi + \phi_0)}{2n} \\ &\times F\{k\rho \sin \beta [1 + \cos(\phi + \phi_0)]\}, \\ P_2 &= \cot \frac{\pi + (\phi - \phi_0)}{2n} - \cot \frac{\pi + (\phi + \phi_0)}{2n}. \end{aligned} \quad (15)$$

$F(x)$ 为UTD过渡函数. 进一步将绕射场写为如下形式:

$$\begin{bmatrix} E_z^d \\ \eta_0 H_z^d \end{bmatrix} = -\mathbf{D} \frac{e^{-jk\rho \sin \beta}}{\sqrt{\rho \sin \beta}} \begin{bmatrix} E_z^i \\ \eta_0 H_z^i \end{bmatrix}. \quad (16)$$

因此可以得到阻抗劈绕射系数矩阵 $\mathbf{D}(\phi, \phi_0, \rho)$ 的元素为

$$\begin{aligned} D_{11} &= -\frac{v_1}{2n} [M_e^0(\alpha_1)P_1 + M_e^0(\alpha_2)P_2], \\ D_{12} &= -\frac{v_1}{2n} [M_e^1(\alpha_1)P_1 + M_e^1(\alpha_2)P_2], \\ D_{21} &= -\frac{v_1}{2n} [M_h^1(\alpha_1)P_1 + M_h^1(\alpha_2)P_2], \\ D_{22} &= -\frac{v_1}{2n} [M_h^0(\alpha_1)P_1 + M_h^0(\alpha_2)P_2], \end{aligned} \quad (17)$$

式中 $v_1 = e^{-j\pi/4} / \sqrt{2\pi k}$, $M_{e,h}^0(\alpha) = \Psi_{e,h}(\alpha) \xi_{e,h}^0(\alpha)$, $M_{e,h}^1(\alpha) = \Psi_{e,h}(\alpha) \xi_{e,h}^1(\alpha) \cos \beta$.

2) 基于掠入射摄动法

由于谱函数的展开项系数 $\varsigma_{T,P}^0(\alpha)$ 及 $\varsigma_{T,P}^1(\alpha)$ 中同时含有电场相关分量 $\varsigma_{T_e,P_e}^0(\alpha)$ 与磁场相关分

量 $\varsigma_{Th,Ph}^1(\alpha)$, 因此需要将其进行分离而变得极为繁琐, 这里仅给出最后的结果.

基于掠入射的阻抗劈绕射系数矩阵 $D(\phi, \phi_0, \rho)$ 的元素为

$$\begin{aligned} D_{11} &= \frac{v_1}{2n} [N_{11}(-\pi + n\pi/2 - \phi)P_1 \\ &\quad + N_{11}(-\pi + n\pi/2 - \phi)P_2], \\ D_{12} &= \frac{v_1}{2n} [N_{12}(\pi + n\pi/2 - \phi)P_1 \\ &\quad + N_{12}(-\pi + n\pi/2 - \phi)P_2], \\ D_{21} &= \frac{v_1}{2n} [N_{21}(\pi + n\pi/2 - \phi)P_1 \\ &\quad + N_{21}(-\pi + n\pi/2 - \phi)P_2], \\ D_{22} &= \frac{v_1}{2n} [N_{22}(\pi + n\pi/2 - \phi)P_1 \\ &\quad + N_{22}(-\pi + n\pi/2 - \phi)P_2], \end{aligned} \quad (18)$$

其中

$$\begin{aligned} N_{11}(\alpha) &= \frac{1}{2} [\Phi_T(\alpha)(\varsigma_{Te}^0(\alpha) - j\varsigma_{Te}^1(\alpha)\sin\beta) \\ &\quad + j\Phi_P(\alpha)(-\varsigma_{Pe}^0(\alpha) + \varsigma_{Pe}^1(\alpha)\sin\beta)], \\ N_{12}(\alpha) &= \frac{1}{2} [\Phi_T(\alpha)(-\varsigma_{Th}^0(\alpha) + \varsigma_{Th}^1(\alpha)\sin\beta) \\ &\quad + j\Phi_P(\alpha)(\varsigma_{Ph}^0(\alpha) - j\varsigma_{Ph}^1(\alpha)\sin\beta)], \\ N_{21}(\alpha) &= \frac{1}{2} [\Phi_P(\alpha)(-\varsigma_{Pe}^0(\alpha) + \varsigma_{Pe}^1(\alpha)\sin\beta) \\ &\quad + j\Phi_T(\alpha)(\varsigma_{Te}^0(\alpha) - j\varsigma_{Te}^1(\alpha)\sin\beta)], \\ N_{22}(\alpha) &= \frac{1}{2} [\Phi_P(\alpha)(\varsigma_{Ph}^0(\alpha) - j\varsigma_{Ph}^1(\alpha)\sin\beta) \\ &\quad + j\Phi_T(\alpha)(-\varsigma_{Th}^0(\alpha) + \varsigma_{Th}^1(\alpha)\sin\beta)]. \end{aligned} \quad (19)$$

$\Phi_{P,T}(\alpha)$ Lyalinov 定义的类似于马丢函数的特殊函数, 具体形式见文献 [16].

2.3 阻抗劈的PO绕射系数

根据边缘波的增量长度绕射系数, 需要扣除 PO 绕射系数的贡献, 因此需要由物理光学场求解出 PO 绕射系数.

在阻抗劈上表面建立局部坐标系如图 2 所示.

入射波和反射波单位矢量分别为

$$\begin{aligned} \hat{k}_i &= (-\hat{x}\sin\beta\cos\phi_0 - \hat{y}\sin\beta\sin\phi_0 + \hat{z}\cos\beta), \\ \hat{s} &= \hat{k}_{sr} = (\hat{x}\sin\beta\cos\phi + \hat{y}\sin\beta\sin\phi + \hat{z}\cos\beta). \end{aligned} \quad (20)$$

用纵向电磁场表示入射电场水平极化分量和垂直

极化分量:

$$\begin{aligned} E_h^i &= \frac{e_z \cos\phi_0 + h_z \cos\beta\sin\phi_0}{\sin\beta\sqrt{1 - \sin^2\beta\sin^2\phi_0}} e^{-jk\cdot\hat{r}'}, \\ E_v^i &= \frac{-e_z \cos\beta\sin\phi_0 + h_z \cos\phi_0}{\sin\beta\sqrt{1 - \sin^2\beta\sin^2\phi_0}} e^{-jk\cdot\hat{r}'}, \end{aligned} \quad (21)$$

其中, e_z 和 h_z 分别为入射电磁场的纵向分量模值.

令 $\hat{\tau} = \hat{n} \times \hat{h}$, 则表面电磁流 (1) 式可化为

$$\begin{aligned} \mathbf{J}(\mathbf{r}') &= \hat{n} \times \mathbf{H} \\ &= \frac{1}{\eta_0} [-(\hat{e}_i \cdot \hat{h})(\hat{n} \cdot \hat{k}_i)(1 - R_{HH})\hat{h} \\ &\quad + (\hat{e}_i \cdot \hat{v})\hat{\tau}(1 + R_{VV})] e^{-jk\hat{k}_i \cdot \mathbf{r}'}, \\ \mathbf{M}(\mathbf{r}') &= \mathbf{E} \times \hat{n} \\ &= -[(\hat{e}_i \cdot \hat{h})(1 + R_{HH})\hat{\tau} \\ &\quad + (\hat{e}_i \cdot \hat{v})(\hat{n} \cdot \hat{k}_i)(1 - R_{VV})\hat{h}] e^{-jk\hat{k}_i \cdot \mathbf{r}'}. \end{aligned} \quad (22)$$

经化简可以得到表面电磁流 x, z 分量为

$$\begin{aligned} J^x &= 2v_2 \sin\phi_0 [\eta_+ \cos\beta \cos\phi_0 e_z \\ &\quad + (\eta_+ \sin\phi_0 + \sin\beta)h_z], \\ J^z &= 2v_2 \sin\phi_0 [(\sin\phi_0 + \eta_+ \cos\beta)e_z \\ &\quad - \cos\beta \cos\phi_0 h_z], \\ M^x &= 2v_2 \sin\phi_0 [-\eta_+(\sin\phi_0 + \eta_+ \sin\beta)e_z \\ &\quad + \cos\beta \cos\phi_0 h_z], \\ M^z &= 2v_2 \sin\phi_0 [\eta_+^2 \cos\beta \cos\phi_0 e_z + \eta_+(\sin\beta \\ &\quad + \eta_+ \sin\phi_0)h_z], \end{aligned} \quad (23)$$

式中, $v_2 = (1 + \eta_+ \sin\beta \sin\phi)^{-1}(\eta_+ + \sin\beta \sin\phi)^{-1}$, $\eta_+ = 1/\sqrt{\epsilon_r}$ 为阻抗面的相对阻抗. 利用修正格林函数, 可以得到由劈表面上的感应电流引起的在 Keller 锥面上的劈面电场及磁场分别为

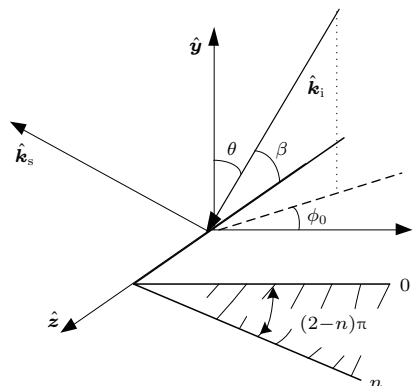


图 2 阻抗劈上表面建立局部坐标系

Fig. 2. Local coordinate system on the up surface of the impedance wedge.

$$\begin{aligned} \mathbf{E}_d^{\text{PO}} &= -\frac{e^{-j\frac{\pi}{4}}}{\sqrt{2\pi k}} \frac{1}{2(\cos\phi + \cos\phi_0)} \frac{e^{-jk_0\rho\sin\beta}}{\sqrt{\rho\sin\beta}} \\ &\cdot (\hat{s} \times \hat{s} \times \mathbf{J} + \hat{s} \times \mathbf{M}), \\ \eta_0 \mathbf{H}_d^{\text{PO}} &= -\frac{e^{-j\frac{\pi}{4}}}{\sqrt{2\pi k}} \frac{1}{2(\cos\phi + \cos\phi_0)} \frac{e^{-jk_0\rho\sin\beta}}{\sqrt{\rho\sin\beta}} \\ &\cdot (\hat{s} \times \hat{s} \times \mathbf{M} - \hat{s} \times \mathbf{J}). \end{aligned} \quad (24)$$

由此得到上劈面的绕射系数为

$$\begin{aligned} D_{11}^{\text{PO}} &= b[-\sin\beta\sin\phi_0 + \eta_+^2\sin\phi\sin\beta \\ &- \eta_+(\sin^2\beta - \sin\phi\sin\phi_0 \\ &- \cos\phi_0\cos\phi\cos^2\beta)], \\ D_{12}^{\text{PO}} &= b[-\eta_+\cos\beta(\sin\phi\cos\phi_0 - \cos\phi\sin\phi_0) \\ &+ \cos\beta\sin\beta(\cos\phi_0 + \cos\phi)], \\ D_{21}^{\text{PO}} &= b[-\eta_+^2\sin\beta\cos\beta(\cos\phi_0 + \cos\phi) \\ &+ \eta_+(\sin\phi\cos\beta\cos\phi_0 \\ &- \cos\phi\cos\beta\sin\phi_0)], \\ D_{22}^{\text{PO}} &= b[\sin\beta\sin\phi_0 - \eta_+^2\sin\phi\sin\beta \\ &- \eta_+(\sin^2\beta - \sin\phi\sin\phi_0 \\ &- \cos\phi_0\cos\phi\cos^2\beta)], \end{aligned} \quad (25)$$

其中 $b = v_1v_2\sin\phi_0/(\cos\phi + \cos\phi_0)$, 下劈面的 PO 绕射系数可由上劈面的绕射系数经 $\eta_+ \rightarrow \eta_-$, $\phi_0 \rightarrow n\pi - \phi_0$, $\phi \rightarrow n\pi - \phi$, $\beta = \pi - \beta$ 变换得到.

2.4 阻抗劈等效边缘电磁流

增量长度绕射系数为 UTD 绕射系数扣除 PO 绕射系数的贡献, 即

$$\mathbf{D}^f = \mathbf{D} - \mathbf{D}^{\text{PO}}. \quad (26)$$

考虑劈边缘等效电磁流为 \mathbf{I}^e 和 \mathbf{I}^m , 它们在 Keller 锥上产生的辐射场为

$$\begin{aligned} E_z^d &= (D_{11}^f E_z^i + D_{12}^f \eta_0 H_z^i) \\ &\times e^{jkz\cos\beta} \frac{e^{jk\rho\sin\beta}}{\sqrt{\rho/\sin\beta}}, \\ \eta_0 H_z^d &= (D_{21}^f E_z^i + D_{22}^f \eta_0 H_z^i) \\ &\times e^{jkz\cos\beta} \frac{e^{jk\rho\sin\beta}}{\sqrt{\rho/\sin\beta}}. \end{aligned} \quad (27)$$

由此可以导出等效边缘电磁流的表达式为

$$\begin{aligned} Z_0 \mathbf{I}^e &= -\frac{e^{j\frac{\pi}{4}} 2\sqrt{2\pi k}}{k} (D_{11}^f E_z^i + D_{12}^f \eta_0 H_z^i) \\ &\times e^{jkz\cos\beta}, \\ \mathbf{I}^m &= -\frac{e^{j\frac{\pi}{4}} 2\sqrt{2\pi k}}{k} (D_{21}^f E_z^i + D_{22}^f \eta_0 H_z^i) \end{aligned}$$

$$\times e^{jkz\cos\beta}. \quad (28)$$

利用电磁流辐射积分公式, 便可以得到等效边缘电磁流的辐射场, 将粗糙面的物理光学场与劈绕射场复数求和即为劈散射总场.

3 数值结果与讨论

以 TE 波为例, 用基于正入射摄动法计算了半平面阻抗劈在平面波斜入射下, 绕射场随散射角的变化(图 3), 并与文献 [13] 给出的精确解结果进行比较. 其中频率 $f = 1$ GHz, $Z_1 = 0.01 - j0.8$, $Z_2 = 0.01 + j2.5$, $\phi_0 = 60^\circ$, $\beta = 98^\circ$. 从图 3 可以看出, 两种方法的电磁场计算结果趋势一致.

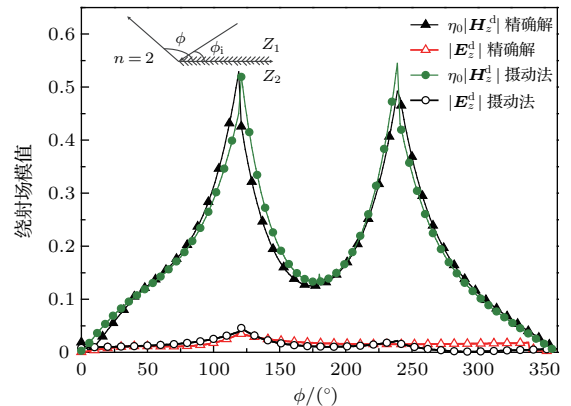


图 3 (网刊彩色) 半平面阻抗劈绕射场

Fig. 3. (color online) Diffracted field from half-plane impedance wedge.

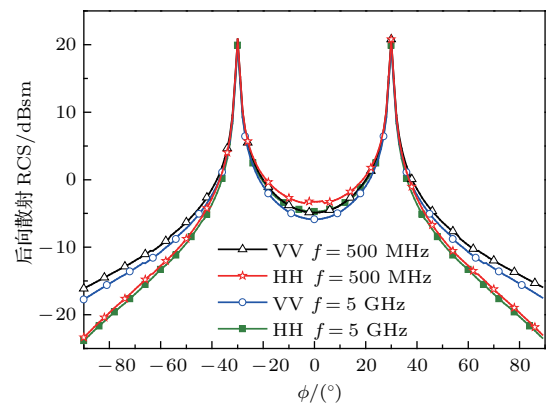


图 4 (网刊彩色) 120° 阻抗劈绕射场后向 RCS

Fig. 4. (color online) Backscattering RCS of the diffracted field from 120° impedance wedge.

图 4 为 120° 阻抗劈在不同频率、不同极化方式下(模型参数与文献 [8] Wedge2 一致) 绕射 RCS 随散射角的变化. 从图 4 可以看出, 垂直于劈尖入射时, HH 极化强于 VV 极化, 而从劈的两侧入射时, HH 极化弱于 VV 极化, 两侧出现的峰值是由于劈

面上的镜面反射造成的, 这与文献[8]中的结论一致。由于海水的介电参数随频率变化, 计算中采用双Debye模型, 因此图4也同时反映了不同的阻抗参数下的绕射场。

图5为不同极化方式下 135° 阻抗劈的绕射场后向RCS随入射角的变化, 模型参数为 $l_1 =$

2 m , $l_2 = 1.41\text{ m}$, $w = 2\text{ m}$, $f = 5\text{ GHz}$ 。从图5可以看出, 135° 阻抗劈在垂直于劈边入射时HH极化大于VV极化, 而在劈边入射时VV极化大于HH极化, 这与 120° 阻抗劈一致。两峰出现在 -30° 及 45° 入射, 这与阻抗劈模型镜像反射对应。图6为物理光学场及用边缘绕射场修正物理光学场后总

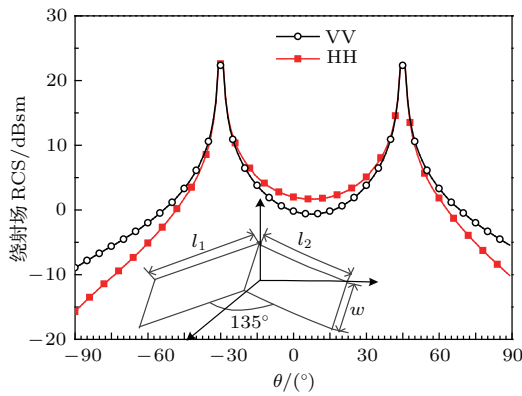


图5 (网刊彩色) 135° 阻抗劈绕射场后向 RCS

Fig. 5. (color online) Backscattering RCS of the diffracted field from 135° impedance wedge.

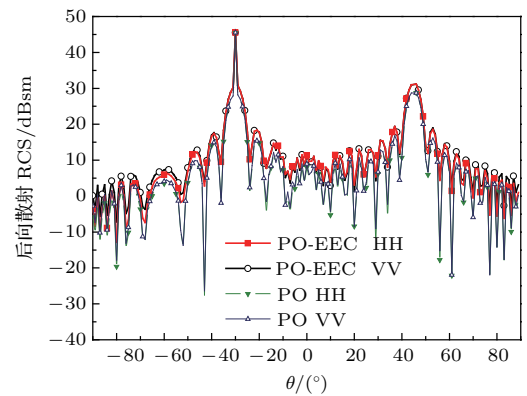
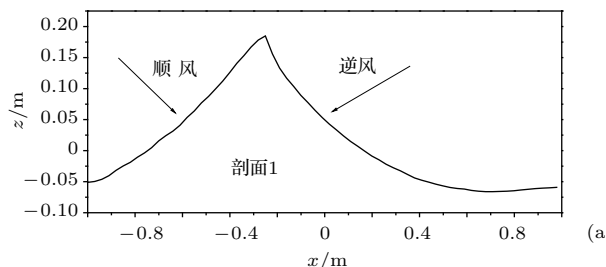
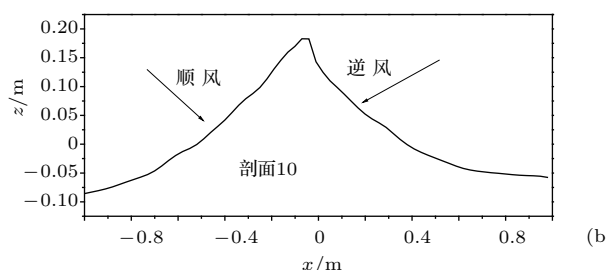


图6 (网刊彩色) 135° 阻抗劈 PO 场及总场后向 RCS

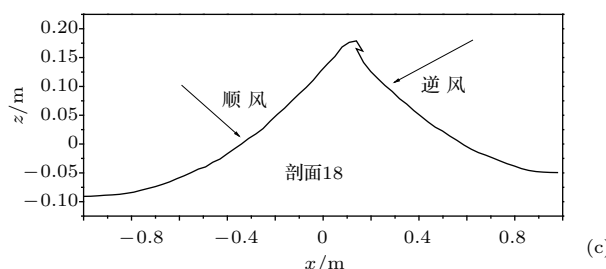
Fig. 6. (color online) Backscattering RCS of PO field and total field from 135° impedance wedge.



(a)



(b)



(c)

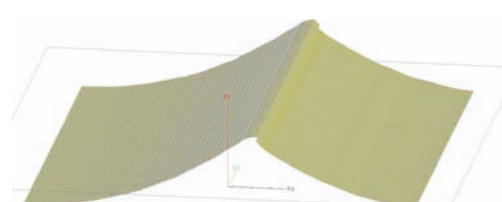
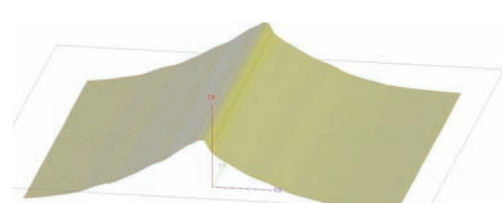


图7 (网刊彩色) LONGTANK 卷浪一维(1D) 及三维(3D) 扩展模型 (a) 第1组剖面; (b) 第10组剖面; (c) 第18组剖面

Fig. 7. (color online) LONGTANK 1D and 3D extended models: (a) Profile 1; (b) profile 10; (c) profile 18.

场随入射角的变化。从图6可以看出,考虑边缘绕射场后,总场值有所增加,特别是在两峰之间,可以看出由于绕射场HH和VV极化的差异,导致HH极化下散射场增加比VV要明显。另外两峰呈现的不对称性主要是由于模型的不对称性造成的。

图7为LONGTANK第1, 10, 18组模型,其参数为 $l = 2$ m, $w = 2$ m, $f = 1$ GHz。由于LONGTANK模型的波面部分平坦,一阶导数连续,可以

认为不含有劈结构,仅考虑物理光学场。波冠部分存在明显的弯折,因此需同时计算物理光学场和劈结构绕射场。在满足剖分精度的前提下,将卷浪模型的波冠看作多个平面劈的组合。从图7可以看出:第1组模型在波冠仅存在一个劈边;第10组模型在波冠两侧存在着两个具有不同外劈角的劈边,而且在逆风侧外劈角较大,其劈绕射场也更大;而第18组剖面由于坍塌作用出现了3个劈边,绕射场为3个劈边的共同作用。

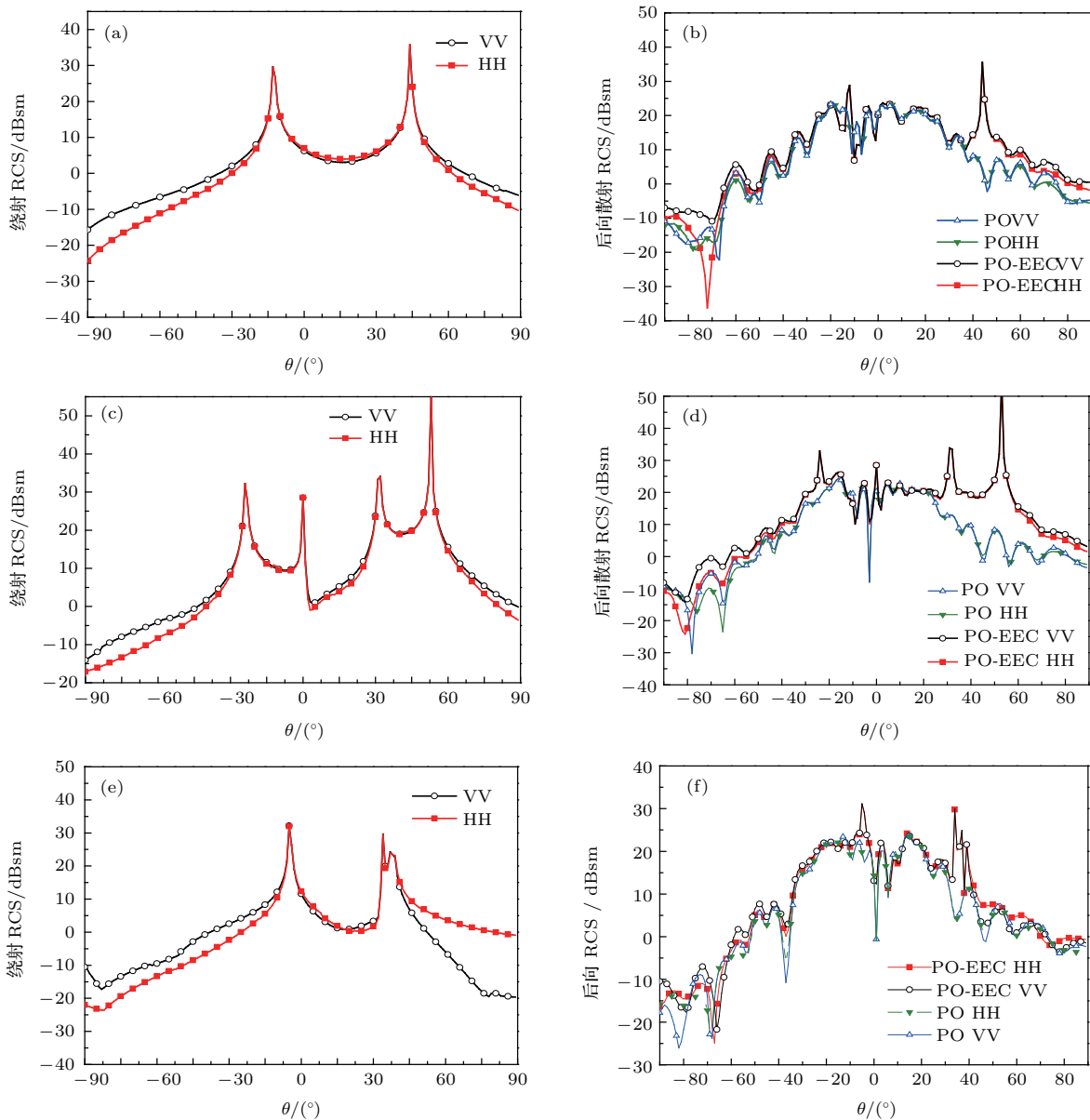


图8 (网刊彩色) LONGTANK 卷浪3D扩展模型散射场后向RCS
(a) 第1组剖面绕射场后向RCS; (b) 第1组剖面PO场及总场后向RCS; (c) 第10组剖面绕射场后向RCS; (d) 第10组剖面PO场及总场后向RCS; (e) 第18组剖面绕射场后向RCS; (f) 第18组剖面PO场及总场后向RCS

Fig. 8. (color online) Backscattering RCS of LONGTANK 3D extended model: (a) Backscattering RCS of the diffracted field of profile 1; (b) backscattering RCS of PO field and total field of profile 1; (c) backscattering RCS of the diffracted field of profile 10; (d) backscattering RCS of PO field and total field of profile 10; (e) backscattering RCS of the diffracted field of profile 18; (f) backscattering RCS of PO field and total field of profile 18.

图8为不同极化方式下三组模型的后向散射系数随入射角的变化。从图8可以看出，在破碎波形成初期(剖面1)，劈边缘绕射场在顺风(约 -13° 入射)和逆风(约 44° 入射)方向出现两个峰值，近似为两个倾斜面的镜像方向。考虑边缘绕射场后，总场值在两峰值附近有明显增加。而随着破碎波的增长(剖面10)，在波冠附近出现了多个峰值，这是由于剖面出现了多个劈边，且总的散射场在劈绕射峰值处有明显增加。破碎波继续生长至坍塌阶段(剖面18)，劈边逐渐向逆风方向坍塌。从图8(e)可以看出，破碎波的劈边绕射场在顺风观测时，VV极化大于HH极化，而逆风小擦地角下，HH极化明显大于VV极化。从图8(f)可以看出，未引入绕射场时顺风条件下的后向散射截面总体上小于逆风的结果，顺风小擦地角条件下HH极化大于VV极化，而逆风条件下HH极化略小于VV极化，这是物理光学场本身的极化差异。绕射场的引入使得顺风条件下HH极化大于VV极化现象减弱，甚至导致部分角度下VV极化总场大于HH极化。而逆风条件下HH极化总场增加明显，出现HH极化大于VV极化的现象。

4 结 论

求解阻抗劈电磁散射，利用摄动法使得计算任意劈结构的散射场成为可能。基于阻抗边界条件，通过阻抗劈绕射的UTD解导出有限长阻抗边缘的等效边缘电磁流，从而以边缘波场合理地修正了物理光学场。建立破碎波3D扩展模型，解决了破碎波散射中阻抗劈绕射场的求解问题。相较于以往导体劈情形，分析了不同频率及介电参数对绕射场的影响，进一步得出当考虑绕射场时，HH极化和VV极化总场后向RCS结果都增大，但顺风下VV极化增大明显，逆风下HH极化增大更明显。从而使得顺风下部分角度VV极化总场大于HH极化的总场，逆风下HH极化总场大于VV极化总场。这

为小擦地角下“海尖峰”出现的原因提供了部分理论依据。

参考文献

- [1] Jessup A T, Keller W C, Melville W K 1990 *J. Geophys. Res.* **95** 9679
- [2] West J C, Sletten M A 1997 *Rad. Sci.* **32** 1455
- [3] Guo L X, Wang R, Wang Y H, Wu Z S 2008 *Acta Phys. Sin.* **57** 3464 (in Chinese) [郭立新, 王蕊, 王运华, 吴振森 2008 物理学报 **57** 3464]
- [4] Kalmykov A I, Pustovoytenko V V 1976 *J. Geophys. Res.* **81** 1960
- [5] Kwoh D, Lake B 1984 *IEEE J. Ocean. Eng.* **9** 291
- [6] Lyzenga D R, Ericson E A 1998 *IEEE Trans. Geosci. Remote Sens.* **36** 636
- [7] Holliday D, DeRaad L L, St-Cyr G J 1996 *IEEE Trans. Antenn. Propag.* **44** 722
- [8] Luo W, Zhang M, Wang C, Yin H C 2011 *Prog. Electromag. Res.* **119** 279
- [9] Wang P, Yao Y, Tulin M P 1995 *Int. J. Numer. Meth. Fluids* **20** 1315
- [10] Li W L, Guo L X, Meng X, Liu W 2014 *Acta Phys. Sin.* **63** 164102 (in Chinese) [李文龙, 郭立新, 孟肖, 刘伟 2014 物理学报 **63** 164102]
- [11] Osipov A V, Norris A N 1999 *Wav. Mot.* **29** 313
- [12] Rojas R G 1988 *IEEE Trans. Antenn. Propag.* **36** 71
- [13] Rojas R G 1988 *IEEE Trans. Antenn. Propag.* **35** 956
- [14] Wu L C, Wang M G 1994 *Chin. J. Rad. Sci.* **9** 76 (in Chinese) [吴良超, 汪茂光 1994 电波科学学报 **9** 76]
- [15] Wu L C, Zhang W X, Wang M G 1996 *Chin. J. Rad. Sci., Special Issue on EMC* 119 (in Chinese) [吴良超, 张文勋, 汪茂光 1996 电波科学学报, 电磁兼容专刊 119]
- [16] Lyalinov M A, Serbest A H, Ikiz T 2001 *International Semina Proceedings of Day on Diffraction* St. Petersburg, Russia, May 29–31, 2001 p180
- [17] Yuan F, Zhu G Q 2005 *Rad. Sci.* **40** 238
- [18] Li J, Zhu G Q, Hu W D 2009 *Chin. J. Rad. Sci.* **24** 761 (in Chinese) [李骥, 朱国强, 胡卫东 2009 电波科学学报 **24** 761]
- [19] Yu D F, He S Y, Fu S 2012 *Sys. Eng. Electron.* **32** 2428 (in Chinese) [余定峰, 何思远, 付松 2012 系统工程与电子技术 **32** 2428]

Effects of impedance wedge diffraction on backscattering from breaking waves*

Zhang Xiao-Xiao¹⁾ Wu Zhen-Sen^{1)2)†} Su Xiang¹⁾

1) (School of Physics and Optoelectronic Engineering, Xidian University, Xi'an 710071, China)

2) (Collaborative Innovation Center of Information Sensing and Understanding, Xidian University, Xi'an 710071, China)

(Received 18 May 2016; revised manuscript received 21 June 2016)

Abstract

Electromagnetic scattering characteristics change significantly from breaking waves, which is considered to be one reason for sea spike phenomenon (HH polarization scattering intensity close to or even greater than VV polarization scattering intensity). Spiky sea clutter is often treated falsely as targets, which affects radar performance in target detection in the sea surface background. Thus the investigation on the physical mechanism of the sea spike phenomenon can help mitigate false alarms. In this paper, the authors investigate the microwave backscattering from the wedge-shaped breaking waves, which is simulated with the dihedral impedance wedge of finite length. The physical optical field of the breaking waves is calculated with the Kirchhoff approximation. Based on the Maliuzhinets method with using the precise impedance boundary condition, the impedance wedge scattering solution in spectral integral representation is presented. The spectral function is derived by the perturbation method with respect to the oblique incident angle based on the incidence normal to or grazing to the edge. After obtaining the spectral function, the asymptotic theory is used to determine the diffraction field of impedance wedge at an arbitrary skew incidence. The equivalent edge currents are derived from the uniform diffraction of impedance wedge by combining the physical optical coefficients and diffracted coefficients. Backscattering radar cross-sections (RCSs) of the diffracted field from 120° impedance wedge are calculated in both HH and VV polarizations, and the effects of frequency and permittivity on the wedge diffraction are discussed as well. The physical optical field backscattering from 135° impedance wedge is compared with the total field with considering the diffraction effects. Further calculations and analyses for backscattering from the three-dimensional extension breaking waves are presented by using the contribution of edge diffraction field to correct the physical optics field. Numerical results show that the backscattering RCS of impedance diffracted field in HH polarization is greater than that in VV polarization in the Keller cone. Therefore, the diffraction effects will make the backscattering RCS of the total field in HH polarization greater than that in VV polarization when the breaking wave grows to near-collapse stage at a small grazing angle with upwind observation. This indicates that the wedge diffraction is one of the causes of sea spike phenomenon.

Keywords: backscattering radar cross-section, breaking waves, impedance wedge, equivalent edge currents

PACS: 41.20.-q, 42.25.Bs, 42.25.Dd

DOI: 10.7498/aps.65.214101

* Project supported by the National Natural Science Foundation of China (Grant No. 61471242).

† Corresponding author. E-mail: Wuzhs@mail.xidian.edu.cn